

Increase in CFC-11 emissions from eastern China based on atmospheric observations

M. Rigby^{1,15}, S. Park^{2,15*}, T. Saito^{3,15}, L. M. Western^{1,15}, A. L. Redington^{4,15}, X. Fang^{5,15}, S. Henne⁶, A. J. Manning⁴, R. G. Prinn⁵, G. S. Dutton^{7,8}, P. J. Fraser⁹, A. L. Ganesan¹⁰, B. D. Hall⁷, C. M. Harth¹¹, J. Kim¹¹, K.-R. Kim², P. B. Krummel⁹, T. Lee², S. Li¹², Q. Liang¹³, M. F. Lunt¹⁴, S. A. Montzka⁷, J. Mühle¹¹, S. O'Doherty¹, M.-K. Park¹², S. Reimann⁶, P. K. Salameh¹¹, P. Simmonds¹, R. L. Tunnicliffe¹, R. F. Weiss¹¹, Y. Yokouchi³ & D. Young¹

The recovery of the stratospheric ozone layer relies on the continued decline in the atmospheric concentrations of ozone-depleting gases such as chlorofluorocarbons¹. The atmospheric concentration of trichlorofluoromethane (CFC-11), the second-most abundant chlorofluorocarbon, has declined substantially since the mid-1990s². A recently reported slowdown in the decline of the atmospheric concentration of CFC-11 after 2012, however, suggests that global emissions have increased^{3,4}. A concurrent increase in CFC-11 emissions from eastern Asia contributes to the global emission increase, but the location and magnitude of this regional source are unknown³. Here, using high-frequency atmospheric observations from Gosan, South Korea, and Hateruma, Japan, together with global monitoring data and atmospheric chemical transport model simulations, we investigate regional CFC-11 emissions from eastern Asia. We show that emissions from eastern mainland China are 7.0 ± 3.0 (± 1 standard deviation) gigagrams per year higher in 2014–2017 than in 2008–2012, and that the increase in emissions arises primarily around the northeastern provinces of Shandong and Hebei. This increase accounts for a substantial fraction (at least 40 to 60 per cent) of the global rise in CFC-11 emissions. We find no evidence for a significant increase in CFC-11 emissions from any other eastern Asian countries or other regions of the world where there are available data for the detection of regional emissions. The attribution of any remaining fraction of the global CFC-11 emission rise to other regions is limited by the sparsity of long-term measurements of sufficient frequency near potentially emissive regions. Several considerations suggest that the increase in CFC-11 emissions from eastern mainland China is likely to be the result of new production and use, which is inconsistent with the Montreal Protocol agreement to phase out global chlorofluorocarbon production by 2010.

Before its global production phase-out in 2010, mandated by the Montreal Protocol on Substances that Deplete the Ozone Layer, CFC-11 was primarily used as an agent for blowing foams that were incorporated into buildings and consumer products. As production declined, it was expected that leakage from banks of CFC-11 stored in these foams would dominate its emissions to the atmosphere. Emissions were projected to decline as these banks depleted¹. However, atmospheric mole fraction data from the US National Oceanic and Atmospheric Administration (NOAA) and the Advanced Global Atmospheric Gases Experiment (AGAGE) show that the rate at which CFC-11 has been declining in the global background atmosphere has slowed since approximately 2013, and its interhemispheric mole fraction difference has increased^{3,4}. Although variations in atmospheric circulation may

have contributed to the slow-down, an increase in northern hemispheric emissions is required, starting after 2012, to explain most of these observed changes³.

High-frequency atmospheric CFC-11 mole fraction data from the AGAGE network⁴ and Japanese National Institute for Environmental Studies (NIES)⁵ show signals that are consistent with a continuing decline in CFC-11 emissions from Europe, North America and Australia in recent years, but a rise from eastern Asia since 2012 (Fig. 1; Extended Data Fig. 1). In these datasets, enhancements above the hemispheric background mole fractions are observed when plumes from nearby sources impinge on the measurement stations. For the AGAGE stations in Europe, the west coast of North America, Australia and more remote locations, the magnitudes of above-baseline events are relatively small and have declined throughout the study period (2008–2017, inclusive), indicating that emissions near these sites have dropped. A decline in emissions from the continental United States has also been inferred over the 2008 to 2014 period with independent NOAA data⁶. By contrast, observations at Hateruma, Japan (see Extended Data Fig. 2 for location), show persistent above-baseline events throughout 2008–2017, which have not declined substantially or may have increased, and data from Gosan, South Korea, show a strong increase in the magnitude of these events after 2012 (Fig. 1). We focus our analysis on eastern Asia because the existing measurement networks only show an increase in the magnitude of above-baseline events in this region. A qualitative emissions increase from somewhere in this region was also indicated in NOAA data from Hawaii³.

To quantify emissions from eastern Asian countries, atmospheric observation-based ‘inverse’ or ‘top-down’ estimates were carried out with CFC-11 measurements from Gosan and Hateruma observations using two atmospheric chemical transport models and four statistical methods (see Methods). Previous top-down studies in this region between 2001 and 2012 had broadly confirmed inventory-based (‘bottom-up’) estimates of declining emissions from China^{7–12}, and found comparatively small emissions from Japan and the Korean Peninsula^{10,13}. Here, we used the NAME¹⁴ and FLEXPART¹⁵ models to simulate the transport of CFC-11 from potential sources to the measurement sites. Emissions were derived from the observed mole fractions using NAME and a hierarchical Bayesian ‘trans-dimensional’ inverse method (denoted NAME-HB)¹⁶ and the Bayesian Inversion Technique for Emissions Modelling (NAME-InTEM)¹⁷. Inversions with FLEXPART used two independent analytical Bayesian frameworks (FLEXPART-MIT¹⁸ and FLEXPART-Empa¹⁹). Analysis using NAME shows that the measurements from the Gosan and Hateruma stations are sensitive to recent emissions from western Japan, the

¹School of Chemistry, University of Bristol, Bristol, UK. ²Department of Oceanography, Kyungpook National University, Daegu, South Korea. ³National Institute for Environmental Studies, Tsukuba, Japan. ⁴Hadley Centre, Met Office, Exeter, UK. ⁵Center for Global Change Science, Massachusetts Institute of Technology, Cambridge, MA, USA. ⁶Empa, Swiss Federal Laboratories for Materials Science and Technology, Dübendorf, Switzerland. ⁷Global Monitoring Division, Earth System Research Laboratory, National Oceanic and Atmospheric Administration, Boulder, CO, USA. ⁸Cooperative Institute for Research in Environmental Sciences, University of Colorado, Boulder, CO, USA. ⁹Climate Science Centre, CSIRO Oceans and Atmosphere, Aspendale, Victoria, Australia. ¹⁰School of Geographical Sciences, University of Bristol, Bristol, UK. ¹¹Scripps Institution of Oceanography, University of California San Diego, La Jolla, CA, USA. ¹²Kyungpook Institute of Oceanography, Kyungpook National University, Daegu, South Korea. ¹³NASA Goddard Space Flight Center, Greenbelt, MD, USA. ¹⁴School of GeoSciences, University of Edinburgh, Edinburgh, UK. ¹⁵These authors contributed equally: M. Rigby, S. Park, T. Saito, L. M. Western, A. L. Redington, X. Fang. *e-mail: sparky@knu.ac.kr

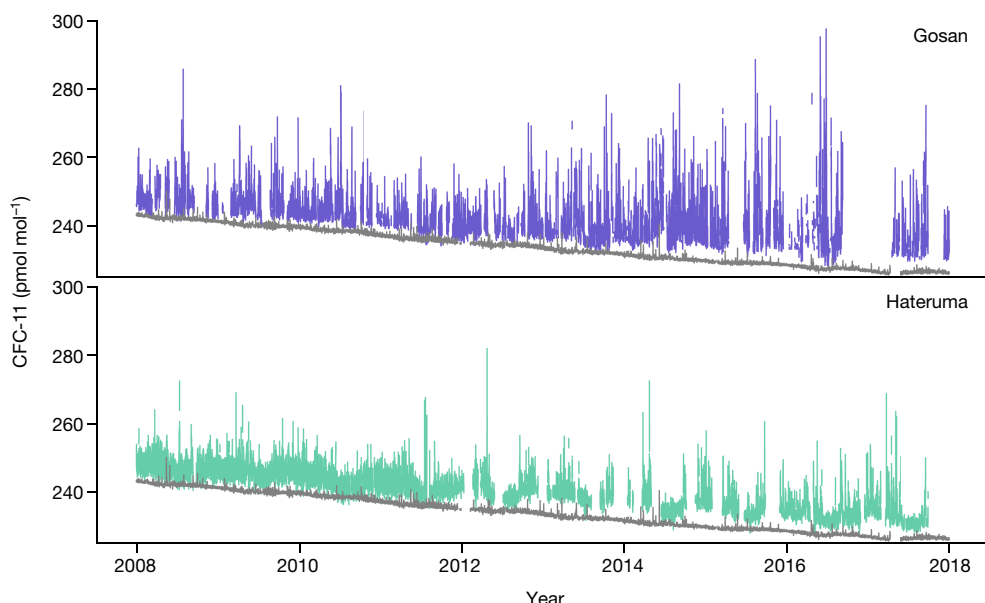


Fig. 1 | Observations of atmospheric CFC-11 at Gosan and Hateruma.

Dry-air mole fractions measured for CFC-11 in discrete air samples at Gosan, Jeju Island, South Korea (33.3° N, 126.2° E) and Hateruma, Japan

(24.1° N, 123.8° E). The grey lines show the mole fraction observations at Cape Grim, Tasmania, Australia (40.7° S, 144.7° E) for comparison.

Korean Peninsula, and a region that we define as ‘eastern mainland China’, which encompasses around 35% of the Chinese population and contains the provinces of Anhui, Beijing, Hebei, Jiangsu, Liaoning, Shandong, Shanghai, Tianjin and Zhejiang (Extended Data Fig. 2). Hence, emissions totals are subsequently provided here only for these eastern Asian regions.

Between 2008 and 2012 (inclusive), we inferred mean CFC-11 emissions of $6.4 \pm 1.2 \text{ Gg yr}^{-1}$ (mean \pm s.d.) for eastern mainland China (Fig. 2; see Methods for details of the technique for estimating multi-inversion mean emissions). The mean derived emission during these years for eastern mainland China is similar to an inventory estimate for the whole of China, when scaled by the fraction of the population that reside in the eastern mainland China region⁷. However, although the inventory-based emission estimates for China show a downward trend during this period, emission magnitudes derived from atmospheric observations did not decline significantly. After 2012, the top-down estimates using four different inverse techniques show an emission increase of CFC-11 from eastern mainland China, although the exact timing of the initial rise differs between inversions. Average emissions between 2014 and 2017 were $13.4 \pm 1.7 \text{ Gg yr}^{-1}$ (for consistency with a previous study, we have omitted 2013 as a transitional year³). Therefore, the increase in derived emissions between the periods 2008–2012 and 2014–2017 is $7.0 \pm 3.0 \text{ Gg yr}^{-1}$, or around 110%. Our top-down inversion-based estimate for CFC-11 emissions from eastern mainland China for 2014–2017 is $8.7 \pm 1.0 \text{ Gg yr}^{-1}$ higher than the population-weighted inventory-based estimate during this period⁷. Together with our inversion-derived emission estimates, the models reproduce the increasing mole fractions during pollution events at the monitoring sites (Extended Data Fig. 3). When using data from either the Hateruma or Gosan sites, a rise in CFC-11 emissions is inferred for eastern mainland China (Extended Data Fig. 4). However, the magnitude of the rise is smaller and more uncertain when using Hateruma alone, probably because measurements at this site are less sensitive to the major emissions sources. The derived emissions are relatively insensitive to the magnitude or distribution of a priori emissions used in the Bayesian inversion frameworks (Extended Data Fig. 5). Emissions derived for western Japan and both countries on the Korean Peninsula are substantially smaller than those derived for eastern mainland China, and the emission magnitudes derived for Japan and Korea did not change significantly during the study period (Extended Data Fig. 6).

To provide context to these eastern Asian emission increases, we provide an update to the global emission magnitudes^{3,4}. Long-term observations of baseline mole fractions, which are representative of air masses that have not been substantially influenced by nearby sources, are used to infer changes in the global emission rate of CFC-11^{3,4}. Using a two-dimensional model of atmospheric transport and chemistry, and assuming a lifetime of 52 years for CFC-11²⁰, we find that $64 \pm 2 \text{ Gg yr}^{-1}$ or $63 \pm 2 \text{ Gg yr}^{-1}$ of CFC-11 were emitted on average between 2008 and 2012 using observations from AGAGE or NOAA, respectively (see Methods; Fig. 2). These emissions increased to a mean value of $75 \pm 3 \text{ Gg yr}^{-1}$ or $80 \pm 3 \text{ Gg yr}^{-1}$ for 2014 to 2017, using AGAGE or NOAA data, respectively, which represents a rise of $11 \pm 3 \text{ Gg yr}^{-1}$ ($17 \pm 5\%$) or $17 \pm 3 \text{ Gg yr}^{-1}$ ($26 \pm 5\%$) above emissions during the 2008–2012 period. Our update shows that the increased global emission rate previously reported for 2014 to 2016^{3,4} persisted in 2017. Consistent with previous studies^{3,4}, our simplified global modelling approach assumes that atmospheric transport did not vary each year, and our uncertainty estimates do not account for the potential influence of yearly changes in atmospheric dynamics on the derived emissions. However, it has been demonstrated that changes in atmospheric transport may have contributed to up to 50% of the slow-down in the rate of decline in the global mole fraction, at least between 2014 and 2016³. Therefore, this inferred average global emission increase, and those that were previously reported, may overestimate the true global emissions rise in recent years.

When compared to the AGAGE-derived or NOAA-derived increase in global emissions, our estimated rise for eastern mainland China accounts for $64 \pm 32\%$ or $41 \pm 20\%$ of the total, respectively. However, given that our increase in global emissions may be overestimated by up to a factor of two, owing to unaccounted-for changes in atmospheric dynamics³, the fraction of the global emission increase accounted for by eastern mainland China may actually be substantially higher. Hence, these results demonstrate that increased emissions from eastern mainland China since 2012 can account for a large fraction of the concurrent rise in global emissions. However, we cannot rule out additional, but probably smaller, increases from other parts of the world (for example, northern, southern and western Asia, Africa and South America), potentially including other parts of China, to which our current measurement networks are insensitive.

The spatial distribution of emissions inferred within our eastern mainland China region for the periods 2008–2012 and 2014–2017

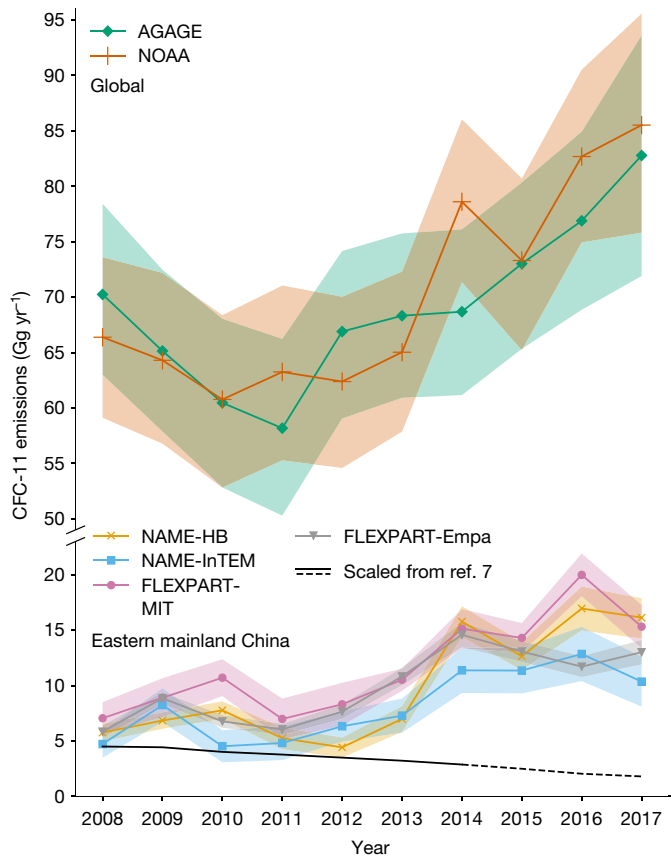


Fig. 2 | CFC-11 emissions derived from atmospheric observations. Top, global emissions estimates derived using a global box model and AGAGE (green diamonds) and NOAA (orange pluses) mole fraction observations of baseline air. Bottom, emissions estimates derived for eastern mainland China using measurements from Gosan (AGAGE, South Korea) and Hateruma (NIES, Japan), and four inverse modelling frameworks: NAME-HB (yellow crosses), NAME-InTEM (blue squares), FLEXPART-MIT (pink circles) and FLEXPART-Empa (grey triangles). Inventory-based estimates for CFC-11 emissions from eastern mainland China (determined as the total Chinese emissions scaled by the fraction of the population, 35%, that reside in that part of the domain) are shown as a solid black line, and a projection of the inventory estimates is shown as a dashed line⁷. All lines and symbols represent the a posteriori mean. Shading denotes the 1 s.d. uncertainty. Global emissions are higher than in a previous study using NOAA data³, because a shorter atmospheric lifetime was used here²⁰.

shows the largest change in or around the provinces of Shandong and Hebei, and to a lesser extent near Shanghai (Fig. 3). This change is evident across all four inversion results (Extended Data Fig. 7). Owing to the effect of atmospheric mixing, and because we used a small number of monitoring stations that are relatively far from the major sources, it is not possible to discern the location of emissions sources at finer scales than provinces, or groups of provinces, in the northeastern part of China. Therefore, it is unclear whether these results indicate that the new emissions originate from a small number of point sources or are more distributed within these regions.

Several factors suggest that the increase in emissions from China is unlikely to originate from increased rates of escape from pre-phase-out banks of CFC-11 in existing foam or refrigerators. First, the spatial distribution of our derived emissions rise is unrelated to population density (Fig. 3), whereas the distribution of banks of foams should be roughly distributed by population. Second, our cumulative emissions from eastern mainland China between 2014 and 2017 (56 ± 7 Gg) are similar to an inventory-based estimate of the CFC-11 bank magnitude for all of China in 2013 (54 Gg)⁷, or almost three times the population-scaled bank for this region, indicating that the bank in 2013

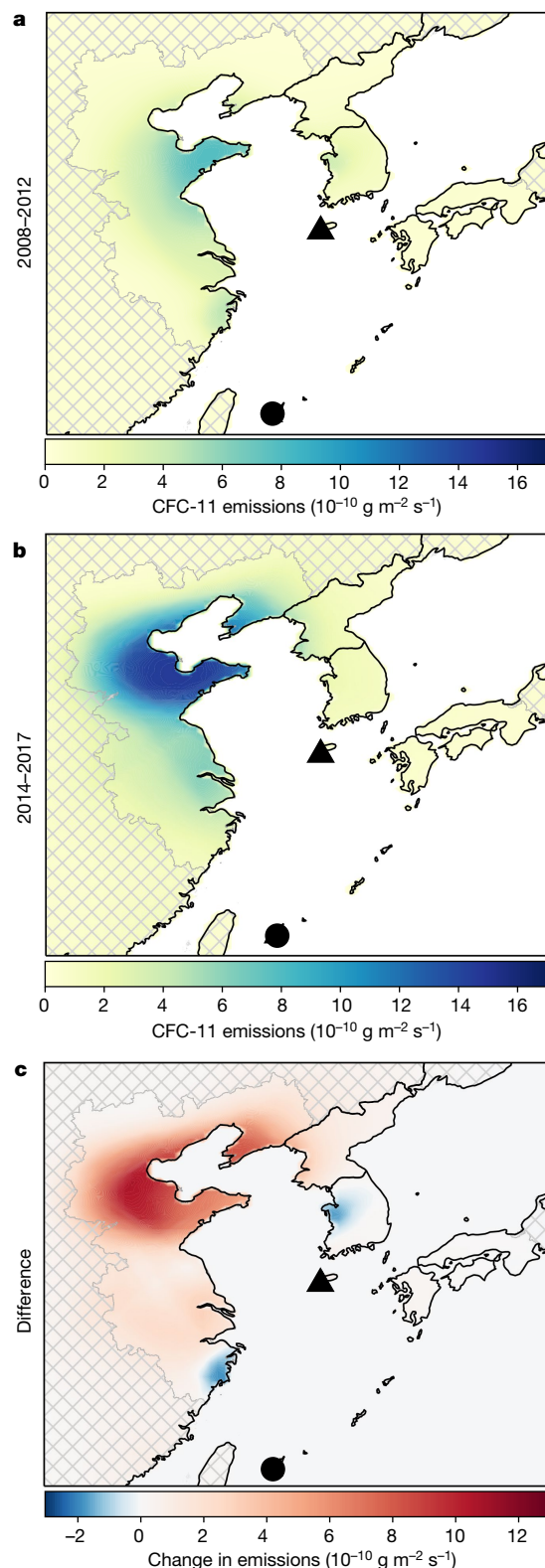


Fig. 3 | Spatial distribution of the derived CFC-11 fluxes in the NAME-HB inversion. a, Mean emissions for 2008–2012. b, Mean emissions for 2014–2017. c, Change in emissions from 2008–2012 to 2014–2017. Equivalent plots for the other inversions are shown in Extended Data Fig. 7. Black triangle and circle indicate the Gosan and Hateruma stations, respectively. The hatched areas indicate regions of the domain to which the observations have low sensitivity (Extended Data Fig. 2), and therefore, from which the derived emissions have high uncertainty. As a result, only emission magnitudes and emission changes for the non-hatched regions are included in the values quoted in the main text.

was not large enough to accommodate the emissions that occurred in subsequent years. Third, even given the possibility that the Chinese bank size was underestimated for 2012, the emission increase derived for eastern mainland China would require the bank release fraction to have increased by around an order of magnitude over the course of five years, a change that seems highly unlikely (Extended Data Fig. 8). To bring about such an increase in the release rate from the bank would require new emissions from the disposal and destruction of refrigerators more than ten times higher than recently estimated for the whole of China between 2014 and 2017²¹, or a larger and more rapid increase in emissions from the demolition of old buildings than was previously predicted for the entire world over a 20-year period (2020–2040)²².

On the basis of this reasoning, it is likely that the new emissions of CFC-11 are the result of new production that has not been reported to the United Nations Environment Programme (UNEP) Ozone Secretariat. Further information is required to confirm which processes are responsible for releasing this newly produced CFC-11 into the atmosphere. If consistent with historical usage, it would be expected that emissions have primarily occurred during, or following, foam blowing, rather than directly during production. Therefore, the regions where emissions have been identified in this study are not necessarily the same as the locations where the compound has been produced. It may be expected that new production of CFC-11 should be accompanied by new emissions of carbon tetrachloride (CCl_4), the starting reagent for the production of CFC-11, and CFC-12 (CF_2Cl_2), which is typically co-produced with CFC-11. Although new emissions of CCl_4 have been identified from parts of eastern China in recent years²³, we do not find evidence for an increase in the emissions of CFC-12 (Extended Data Fig. 9). Given the different historical uses of CFC-11 and CFC-12 (primarily in foam blowing and refrigeration, respectively), the relationship between production and the subsequent rate of emission may also be very different for these two substances. Therefore, the lack of a detectable increase in CFC-12 emissions does not preclude a recent rise in CFC-11 production.

Our results show that new CFC-11 emissions from eastern mainland China explain a substantial fraction of the post-2012 rise in global emissions, and are probably due to new, unreported production and use. It is important to recall that before this period, global emissions had not declined as expected since the early 2000s, and by 2012 were around 10 Gg yr^{-1} higher than projections³. In contrast to the recent rise, we propose that emissions from eastern mainland China are unlikely to have contributed substantially to this earlier ‘plateau’, because our derived emissions for this region during 2008 to 2012 are relatively small ($6.4 \pm 1.2 \text{ Gg yr}^{-1}$) and are consistent with the estimated release rates from banks⁷. Other countries, and indeed the rest of China, which are not well observed by the current monitoring networks may also have contributed to the unexpected trends in CFC-11, which have now been ongoing for almost two decades. Further investigation will be required to determine which processes have led to the inferred recent increase in emissions from China (and potentially elsewhere) and the magnitude of any associated, unreported CFC-11 production. Depending on which processes are responsible, the new emissions may represent only a fraction of the total new production, with the remainder contained in more slowly emitting banks (for example, foams). Ultimately, because nearly all known uses of CFC-11 are dispersive, it is the total production magnitude that will determine the overall effect of these activities on the ozone layer and its recovery.

Online content

Any methods, additional references, Nature Research reporting summaries, source data, statements of data availability and associated accession codes are available at <https://doi.org/10.1038/s41586-019-1193-4>.

Received: 15 November 2018; Accepted: 2 April 2019;

Published online 22 May 2019.

- Harris, N. R. P. & Wuebbles, D. J. in *Scientific Assessment of Ozone Depletion: 2014 Ch. 5*, 416 (World Meteorological Organization, 2014).

- Carpenter, L. J. & Reimann, S. in *Scientific Assessment of Ozone Depletion: 2014 Ch. 1* (World Meteorological Organization, 2014).
- Montzka, S. A. et al. An unexpected and persistent increase in global emissions of ozone-depleting CFC-11. *Nature* **557**, 413–417 (2018).
- Prinn, R. G. et al. History of chemically and radiatively important atmospheric gases from the Advanced Global Atmospheric Gases Experiment (AGAGE). *Earth Syst. Sci. Data* **10**, 985–1018 (2018).
- Yokouchi, Y. et al. High frequency measurements of HFCs at a remote site in east Asia and their implications for Chinese emissions. *Geophys. Res. Lett.* **33**, L21814 (2006).
- Hu, L. et al. Considerable contribution of the Montreal Protocol to declining greenhouse gas emissions from the United States. *Geophys. Res. Lett.* **44**, 8075–8083 (2017).
- Fang, X. et al. Changes in emissions of ozone-depleting substances from China due to implementation of the Montreal Protocol. *Environ. Sci. Technol.* **52**, 11359–11366 (2018).
- Palmer, P. I. et al. Eastern Asian emissions of anthropogenic halocarbons deduced from aircraft concentration data. *J. Geophys. Res. Atmos.* **108**, 4753 (2003).
- An, X. et al. Estimating emissions of HCFC-22 and CFC-11 in China by atmospheric observations and inverse modeling. *Sci. China Chem.* **55**, 2233–2241 (2012).
- Li, S. et al. Emissions of halogenated compounds in East Asia determined from measurements at Jeju Island, Korea. *Environ. Sci. Technol.* **45**, 5668–5675 (2011).
- Kim, J. et al. Regional atmospheric emissions determined from measurements at Jeju Island, Korea: halogenated compounds from China. *Geophys. Res. Lett.* **37**, L12801 (2010).
- Vollmer, M. K. et al. Emissions of ozone-depleting halocarbons from China. *Geophys. Res. Lett.* **36**, L15823 (2009).
- Saito, T. et al. Extraordinary halocarbon emissions initiated by the 2011 Tohoku earthquake. *Geophys. Res. Lett.* **42**, 2500–2507 (2015).
- Manning, A. J., O'Doherty, S., Jones, A. R., Simmonds, P. G. & Derwent, R. G. Estimating UK methane and nitrous oxide emissions from 1990 to 2007 using an inversion modeling approach. *J. Geophys. Res.* **116**, D02305 (2011).
- Stohl, A., Forster, C., Frank, A., Seibert, P. & Wotawa, G. Technical note: the Lagrangian particle dispersion model FLEXPART version 6.2. *Atmos. Chem. Phys.* **5**, 2461–2474 (2005).
- Lunt, M. F., Rigby, M., Ganeshan, A. L. & Manning, A. J. Estimation of trace gas fluxes with objectively determined basis functions using reversible-jump Markov chain Monte Carlo. *Geosci. Model Dev.* **9**, 3213–3229 (2016).
- Arnold, T. et al. Inverse modelling of CF4 and NF3 emissions in East Asia. *Atmos. Chem. Phys.* **18**, 13305–13320 (2018).
- Fang, X. et al. Rapid increase in ozone-depleting chloroform emissions from China. *Nat. Geosci.* **12**, 89–93 (2019).
- Henne, S. et al. Validation of the Swiss methane emission inventory by atmospheric observations and inverse modelling. *Atmos. Chem. Phys.* **16**, 3683–3710 (2016).
- Ko, M. K. W., Newman, P. A., Reimann, S. & Strahan, S. E. in *SPARC Report No. 6: Lifetimes of Stratospheric Ozone-Depleting Substances, Their Replacements, and Related Species* (eds Ko, M. et al.) (Stratospheric Processes And their Role in Climate, 2013).
- Duan, H. et al. Chilling prospect: climate change effects of mismanaged refrigerants in China. *Environ. Sci. Technol.* **52**, 6350–6356 (2018).
- The Intergovernmental Panel on Climate Change. *Safeguarding the Ozone Layer and the Global Climate System: Issues Related to Hydrofluorocarbons and Perfluorocarbons (SROC)* (IPCC/TEAP, Cambridge Univ. Press, 2005).
- Lunt, M. F. et al. Continued emissions of the ozone-depleting substance carbon tetrachloride from eastern Asia. *Geophys. Res. Lett.* **45**, 11423–11430 (2018).

Acknowledgements We are indebted to the site operators who oversee the day-to-day running of the AGAGE, NIES and NOAA stations. We particularly thank the NASA Upper Atmosphere Research Program for its continuing support of AGAGE, including providing modelling, field station and instrumentation support through grant NNX16AC98G to MIT, and supporting the overall experimental programme through grants NNX16AC96G and NNX16AC97G to SIO. Observations at Cape Grim are supported largely by the Australian Bureau of Meteorology, CSIRO, the Australian Department of the Environment and Energy (DoEE) and Refrigerant Reclaim Australia (RRA). Mace Head, Ireland, is supported by the Department for Business, Energy & Industrial Strategy (BEIS, UK, formerly the Department of Energy and Climate Change (DECC)) contract 1028/06/2015 to the University of Bristol and the UK Meteorological Office. Ragged Point, Barbados is supported by the National Oceanic and Atmospheric Administration (NOAA, USA), contract RA-133-R15-CN-0008 to the University of Bristol. M.R., L.M.W., M.F.L. and R.L.T. were supported by Natural Environment Research Council grants NE/I021365/1, NE/I027282/1, NE/M014851/1, NE/L013088/1 and NE/N016548/1. A.L.G. is supported by NERC Independent Research Fellowship NE/L010992/1. S.P., T.L., S.L., M.-K.P. and K.-R.K. were supported by Basic Science Research Program through the National Research Foundation of Korea (NRF) funded by the Ministry of Education (no. NRF-2016R1A2B2010663). Observations at Hateruma were partly supported by the Ministry of the Environment of Japan. S.A.M., B.D.H. and G.S.D. are indebted to C. Siso, D. Mondeel, J. D. Nance, F. Moore, J.W. Elkins, B. Vasel, C. Schultz, R. Schnell and J. H. Butler for discussions and assistance with the NOAA measurements considered here, which were made possible in part with support from the NOAA Climate Program Office's AC4 program.

Reviewer information *Nature* thanks Andreas Stohl, Guus Velders and the other anonymous reviewer(s) for their contribution to the peer review of this work.

Author contributions S.P., T.S., G.S.D., P.J.F., B.D.H., C.M.H., J.K., K.-R.K., P.B.K., T.L., S.L., S.A.M., J.M., S.O., M.-K.P., P.K.S., P.S., R.F.W., Y.Y. and D.Y. contributed observational data. L.M.W., A.L.R., X.F. and S.H. carried out atmospheric model simulations and inverse analysis with support from R.L.T., M.F.L. and A.L.G., and under the supervision of M.R., A.J.M., S.R. and R.G.P. All authors wrote the manuscript.

Competing interests The authors declare no competing interests.

Additional information

Extended data is available for this paper at <https://doi.org/10.1038/s41586-019-1193-4>.

Supplementary information is available for this paper at <https://doi.org/10.1038/s41586-019-1193-4>.

Reprints and permissions information is available at <http://www.nature.com/reprints>.

Correspondence and requests for materials should be addressed to S.P.

Publisher's note: Springer Nature remains neutral with regard to jurisdictional claims in published maps and institutional affiliations.

© The Author(s), under exclusive licence to Springer Nature Limited 2019

METHODS

Data. Atmospheric mole fraction observations were made at a frequency of around 34 measurements per day at the remote AGAGE stations using gas chromatography-electron capture detection (GC-ECD)⁴. These stations are at Mace Head, Ireland (53.3° N, 9.9° W), Trinidad Head, California, USA (41.1° N, 124.2° W), Ragged Point, Barbados (13.2° N, 59.4° W), Cape Matatula, American Samoa (14.2° S, 170.7° W) and Cape Grim, Tasmania, Australia (40.7° S, 144.7° E). At the AGAGE station at Gosan, South Korea (33.3° N, 126.2° E), around 12 measurements were made each day using gas chromatography-mass spectrometry (GC-MS)²⁴. Measurements at the NIES, AGAGE-affiliate station at Hateruma, Japan (24.1° N, 123.8° E), were made at a frequency of around 20 measurements per day using GC-MS²⁵. AGAGE measurements are reported on the Scripps Institution of Oceanography (SIO) 2005 scale and NIES measurements are reported on the NIES-08 scale. Hateruma data were converted to the SIO-05 scale by multiplying by an intercalibration factor of 0.996, determined through exchange of air samples. The estimated repeatability of the Hateruma data was approximately 0.8%, and the average repeatability of the Gosan data was approximately 0.2%, although this varies throughout the time series. Measurements are reported throughout as a dry air mole fraction in moles of CFC per 10¹² mole air (pmol mol⁻¹).

The NOAA background atmospheric CFC-11 measurements from three different methods were combined into a single atmospheric history for this analysis (for the combined record, see <ftp://ftp.cmdl.noaa.gov/hats/cfcs/cfc11/combined/> for data and <https://www.esrl.noaa.gov/gmd/hats/combined/CFC11.html> for a description of the methodology). Those methods include GC-ECD measurements at hourly frequency using on-site instrumentation, and the GC-ECD and GC-MS (the latter included only since 2010) analysis of glass and stainless-steel flasks collected approximately weekly at 12 locations across the globe. Flasks were analysed in Boulder, Colorado, USA³. NOAA data are reported using the NOAA-2016 scale.

Differences between the NOAA-2016 and the SIO-05 scales are 1% or less⁴. Therefore, differences between the AGAGE-derived and NOAA-derived global emissions (Fig. 2) are not strongly influenced by calibration differences. Global inversions were carried out using AGAGE and NOAA data on their respective calibration scales. Uncertainties due to inaccuracies in the calibration scales were not included in the global emissions estimates (see below).

Regional atmospheric chemical transport models. We use two backward-running Lagrangian chemical transport models to estimate the sensitivity of the atmospheric observations to fluxes in the eastern Asian region: NAME¹⁴ and FLEXPART¹⁵. Both models simulate transport of CFC-11 by advection and random diffusion, by atmospheric turbulence, of hypothetical particles of the gas. The 'footprint' of each measurement, calculated from these simulations, describes the sensitivity of the observation to emissions from surrounding model grid cells (Extended Data Fig. 2). A comparison of the simulated and observed data is shown in Extended Data Fig. 3.

NAME was driven by meteorological fields from the UK Met Office Unified Model²⁶, the spatial resolution of which increased in the study period from 0.563° to 0.141° longitude and 0.375° to 0.094° latitude, whereas the temporal resolution has remained fixed at 3 h. Approximately 20,000 particles per hour were transported backward in time for 30 days in NAME in a domain bounded at 5° S and 74° N and 55° E and 192° E. When particles are within the lowest 40 m of the atmosphere, it was assumed that they interacted with the surface and could intercept emissions sources^{17,23}. The NAME-HB framework uses a climatological a priori estimate of the mole fraction at the boundary of the domain from the NASA 3D GEOS Chemistry Climate Model²⁷. By contrast, the NAME-InTEM inversion estimated the baseline mole fraction at each measurement station (see below).

FLEXPART was run in different modes by the MIT and Empa groups. FLEXPART-Empa released 50,000 particles in each 3-h interval and traced them backwards in time for 10 days, driven by operational ECMWF analysis with 1° × 1° global resolution and 0.2° × 0.2° resolution for northeastern China (105° E to 125° E and 30° N to 50° N). FLEXPART-MIT released 40,000 particles in each 3-h interval and traced them backwards in time for 20 days in a global domain, driven by operational ECMWF analysis at 1° × 1° global resolution.

Regional inversion frameworks. Fluxes were derived using four different Bayesian inversion frameworks. Bayesian inverse modelling systems use an a priori estimate of emissions, which, when combined with chemical transport models, can be subsequently updated to bring the models into consistency with observations. In our study, different a priori estimates were used in each regional inversion, although in every case these estimates primarily served to weakly limit the spatial area from which emissions were inferred (they were limited to being over land, but not further constrained to any particular land-based regions), and to provide the inversion with an approximate magnitude for the fluxes (by typically being some fraction of the global total). The magnitude of the a priori emissions was constant for each year of the study, so that any temporal variation in the a posteriori emissions was driven only by the data. Bayesian frameworks require that some uncertainty is

placed on these prior estimates along with an estimate of the model-measurement uncertainty covariance (see below). The hierarchical approach allows these uncertainty factors, along with other parameters, to be estimated in the inversion²⁸. Our inversions were shown to be relatively insensitive to the choice of a prior emissions magnitude or distribution (Extended Data Fig. 5).

The trans-dimensional hierarchical Bayesian inversion used with NAME footprints (NAME-HB) estimates the model-measurement uncertainty in the inversion²⁸. Furthermore, the level of spatial disaggregation of the emissions field can also be explored¹⁶. This scheme is solved using reversible-jump Markov chain Monte Carlo (rj-MCMC)²⁹. The inversion is split into an inner domain (74° W to 160° W, 22° N to 50° N), where spatial disaggregation can occur, and an outer domain split into four fixed regions to the North, South, East and West extending to the boundary of the NAME domain. Emissions are estimated at variable resolution (determined by the rj-MCMC algorithm) in the inner domain and from the four fixed regions outside this domain. Simultaneously, boundary conditions at the four domain edges were solved for by scaling the a priori mole fraction fields at these edges. The NAME-HB a priori estimate of CFC-11 emissions were 20 Gg yr⁻¹ distributed uniformly over land (not water) in the inner domain and a further 20 Gg yr⁻¹ in the outer domain, meaning that the combined domain accounts for roughly two-thirds of global emissions. This results in national a priori emissions estimates of 17.3 Gg yr⁻¹ for China (5.5 Gg yr⁻¹ for eastern mainland China) and 1.2, 0.31 and 0.42 Gg yr⁻¹ for Japan, South Korea and North Korea, respectively. Within each country, these prior fluxes were uniformly distributed in space. The uncertainty on these flux estimates was assumed to be log-normally distributed, with the mode fixed to the a priori estimated emission and a logarithmic standard deviation of 10, defined as the square-root of the ratio of the exponential of the mean to the mode. Model uncertainties are informed by the data in the hierarchical framework. The model error was assumed to be normally distributed with zero mean and a standard deviation that was allowed to vary, with equal probability, between 1 and 20 pmol mol⁻¹, with an autocorrelation timescale between 1 and 120 h. The measurement data and footprints were averaged into daily values, with a fixed measurement uncertainty equal to the repeatability of the raw measurements plus the variability of the measurements within the daily averaging period (a measure of the sub-daily fluctuations that would not be resolved by the inversion). Emissions were assumed constant throughout the year, and emissions and monthly boundary condition scaling factors were estimated independently within each year.

Output from NAME was also used with the InTEM inversion framework (NAME-InTEM)¹⁷. A priori CFC-11 estimates were given large uncertainties, namely 22 (0–147) Gg yr⁻¹ for China, 5 (0–35) Gg yr⁻¹ for eastern mainland China, and 2 (0–20), 0.3 (0–3.2) and 0.4 (0–3.8) Gg yr⁻¹ for Japan, South Korea and North Korea, respectively. This is based on 50 Gg yr⁻¹ uniformly emitted across the whole eastern Asian land area. Observational uncertainty was time varying and was estimated as the variability of the observations in a 6-h moving window plus the measurement repeatability determined from repeat measurements of the on-site calibration standards. Model uncertainty was estimated every 2 h as the larger of the median of all pollution events at each station in a year or 16.5% of the magnitude of the pollution event. A temporal correlation of 12 h was assumed in the model uncertainty at each station. An analytical solution was found that minimized the residual between the model and the observations and the difference between the posterior and prior flux estimate, balanced by the uncertainties of both. The mole fraction baseline at each station was estimated in the inversion described previously¹⁷. The variable resolution of the inversion grid was calculated and refined within InTEM based on the magnitude of the footprint and emissions from each grid box. The inversions were run several (24) times per year, each time with a randomly generated sub-sample (90%) of the available observations (10% removed in 5-day blocks), to further explore the uncertainty. Emissions and uncertainties were averaged across the 24 individual inversions thereby assuming 100% correlation between uncertainties in these separate inversions.

The FLEXPART-MIT inversion derived fluxes using FLEXPART with an analytical Bayesian framework³⁰. Prior flux fields were set to be spatially uniform over continental eastern Asia. Emissions were solved within variable-resolution grid cells with the finest grid (1° × 1°) in eastern China and other eastern Asian countries³¹. A priori estimates of CFC-11 flux were 14.5 Gg yr⁻¹ for China (1.5 Gg yr⁻¹ for eastern mainland China) and 1.2, 0.27 and 0.27 Gg yr⁻¹ for Japan, South Korea and North Korea, respectively. The uncertainty on each grid cell was arbitrarily set to 1,000% and the spatial correlation length was assumed 300 km, so that the total a priori emission uncertainty for China, for example, was 43.2 Gg yr⁻¹. Baseline mole fractions were estimated at each site every 7 days³¹. Model-measurement uncertainty for each 24-h-averaged observation was estimated as the quadratic sum of 1% of the baseline value (as a measure of baseline uncertainty), the measurement repeatability and the standard deviation of the 24-hourly variability (as a measure of the model-data 'mismatch' uncertainty). Similar to InTEM, a posteriori fluxes were derived using an analytical approach that minimizes a cost

function that weights the measurement-model residuals and the a priori estimate by their respective uncertainties.

Fluxes were derived with a second FLEXPART-based approach but using the FLEXPART-Empa simulations and an alternative analytical Bayesian framework¹⁹. Prior fluxes were set to a homogeneous value over all land areas with total Chinese and eastern mainland Chinese emissions of 14.9 Gg yr^{-1} and 2.7 Gg yr^{-1} , respectively, ($0.66, 0.18, 0.22 \text{ Gg yr}^{-1}$ for Japan, South Korea and North Korea). Observations were aggregated to 3-hourly averages to derive gridded annual mean emissions. The baseline was optimized as part of the state vector, independently for both sites. No a priori covariance between emissions and baseline were assigned. Parameters describing the covariance structure of the data-mismatch uncertainty matrix and the a priori uncertainty matrix were estimated using a maximum likelihood approach¹⁹. These parameters include an estimate of the model uncertainty at the individual sites, the a priori baseline uncertainty and its temporal correlation length scale, a domain-total a priori uncertainty, and a spatial correlation length scale. The domain-total a priori uncertainty was estimated to range from $\pm 45\%$ (in 2008) to $\pm 125\%$ (in 2016), which translates to a regional a priori uncertainty of $\pm 100\%$ to $\pm 270\%$ for the eastern mainland China region.

Where the emissions, derived from multiple regional inversions and multiple years, were combined, we took the mean of the a posteriori annual inversion means. Mean emissions are calculated throughout the text for the periods 2008–2012 and 2014–2017 (inclusive). The year 2008 was used to bound the first averaging period, when a whole year of Gosan data first became available. A previous study³, which estimated global emissions using NOAA data, omitted the year 2013, because global emissions in this year appeared to be intermediate between two periods of more constant emission. While our estimates, which use multiple models and measurement networks, are less clear on whether such an intermediate period occurred, we also omit the year 2013, so that our estimates can be more directly compared with this previous work. Uncertainties in the multi-inversion means were calculated from the a posteriori uncertainty from the individual models and years, assuming that these uncertainties were fully correlated (that is, assuming that the different inversions did not provide statistically independent estimates of emissions). The latter assumption attempts to account for the fact that the inversions share the same models, which will suffer from similar systematic uncertainties (in the case of the two NAME inversions or two FLEXPART inversions). Such systematic uncertainties are not explored in any of the inversion frameworks and are therefore not reflected in the individual a posteriori emission estimates. Therefore, the individual uncertainty estimates are likely to be underestimates of the full uncertainty (as seen by the non-overlapping uncertainties in some years in, for example, Fig. 2). It is also possible that, for the same reason, our multi-inversion uncertainty is an under-estimate.

On the basis of a consideration of the sensitivity of the observations to potential sources that surround the measurement sites (note that the NOAA and AGAGE network currently have a limited number of stations that are close enough to industrialized regions for the detection of regional emission sources), we have opted to focus on the total emissions rise from a region that we denote eastern mainland China (Extended Data Fig. 2, a similar sub-division was also used for western Japan). Further away from this region, atmospheric mixing of plumes that emanate from emissions sources makes their effect on the observations small, compared to measurement and modelling uncertainty (which is why the existing, sparse network is insensitive to large parts of the globe). The choice of which Chinese provinces to include in this region was subjective, and could alter the derived rise in emissions and associated uncertainty. For example, inclusion of the provinces adjacent to our eastern mainland China region (excluding the very large Inner Mongolia) would lead to an increase of approximately 15% in the emissions rise derived between 2008–2012 and 2014–2017. However, the associated uncertainty increased by around 30%. We note that the use of a larger region would explain a larger (but more uncertain) fraction of the global emissions rise than obtained from the eastern mainland China region alone.

Global average emissions estimation. Global emissions were estimated from AGAGE or NOAA data with a least-squares method used previously for estimation of global CFC-11 emissions³. Monthly mean baseline-filtered observations³² from the five remote AGAGE stations or the NOAA flask and in situ sites were averaged into semi-hemispheres, separated at the equator and 30° north or south (NOAA data were weighted by the sine of their latitude within each semi-hemisphere). Mole fractions were simulated for each semi-hemisphere using a 12-box model of the atmosphere with vertical divisions at 500 hPa and 200 hPa³³. Seasonally

varying, yearly repeating advection and diffusion parameters were used to transport CFC-11 between model boxes. Loss was assumed only to occur in the stratospheric boxes, at a rate that was adjusted to provide a global mean steady-state lifetime of 52 years²⁰. Uncertainties related to the ability of the model to simulate the data consisted of the sum of two factors. The first term, equal to the baseline variability in each month determined by the AGAGE network, was assumed to be a measure of the temporal representation error between the model and the data. A second fixed uncertainty (0.3%), equal to the approximate level of disagreement between the AGAGE and NOAA monthly semi-hemispheric means, was used to parameterize spatial and temporal differences in the sampling between the networks and uncertainties in the propagation of calibration scales to the sites. These uncertainties are propagated through to the emissions estimates. However, our estimates do not include an uncertainty contribution due to calibration scale uncertainty or atmospheric lifetime uncertainty³³. These terms are important for quantifying the absolute derived emissions values but have little influence on the change in emissions between time periods, which is the primary focus of this paper. Similarly to previous studies^{3,4}, our uncertainties do not include a contribution due to the assumption of yearly repeating dynamics. To estimate the implications of this assumption would require three-dimensional global model simulations, which were not available for this work.

Reporting summary. Further information on research design is available in the Nature Research Reporting Summary linked to this paper.

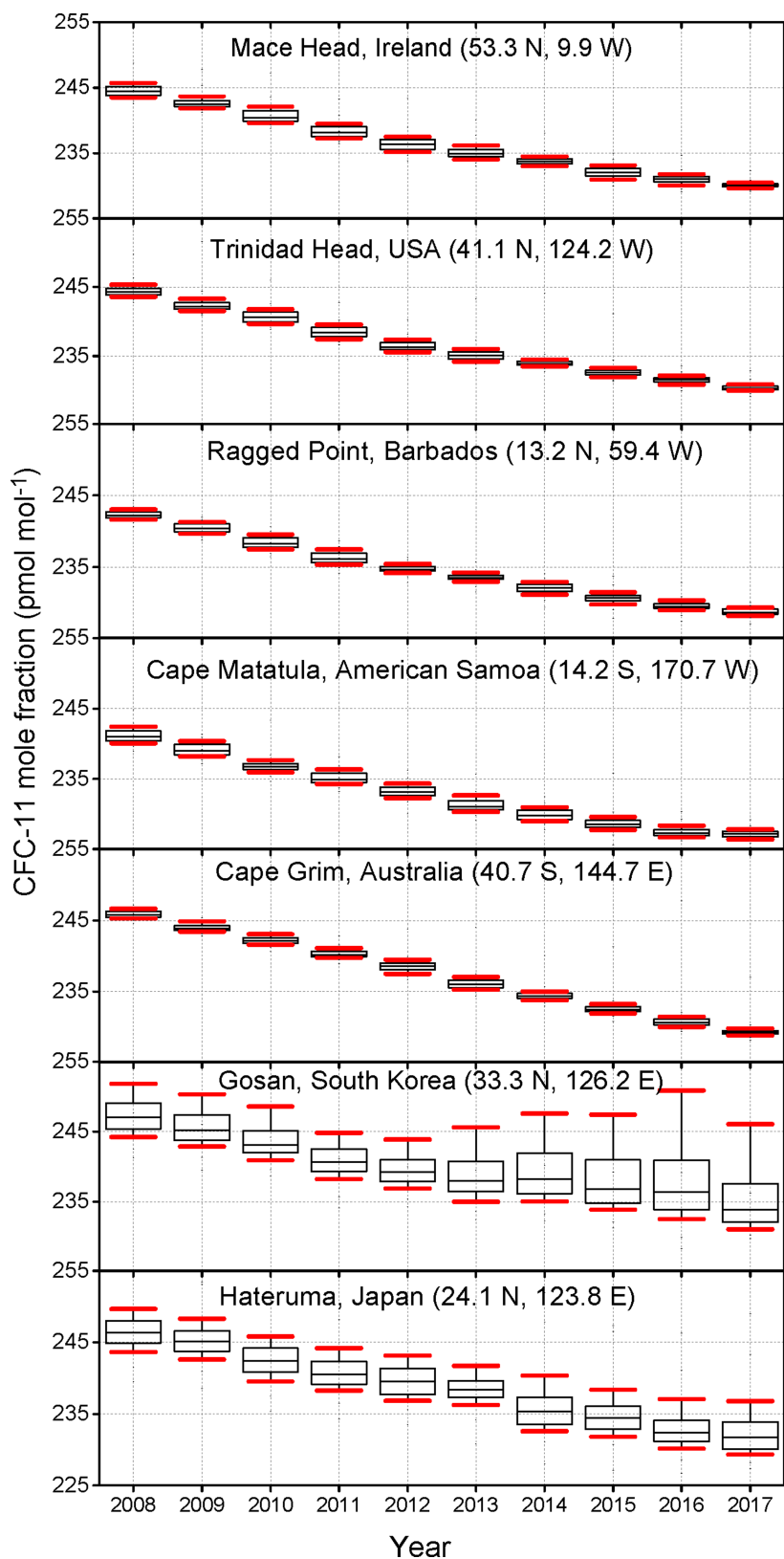
Data availability

Data from remote AGAGE stations and Gosan data are available from the AGAGE website (agage.mit.edu). Hateruma data are available at World Data Centre for Greenhouse Gases (<https://gaw.kishou.go.jp/>). NOAA data are taken as the ‘combined set’ data record (a best-estimate record based on flask samples and in situ measurements), available from the NOAA Global Monitoring Division data server (<https://www.esrl.noaa.gov/gmd/dv/ftpdata.html>, or more specifically <ftp://ftp.cmdl.noaa.gov/hats/cfc11/combined/>).

Code availability

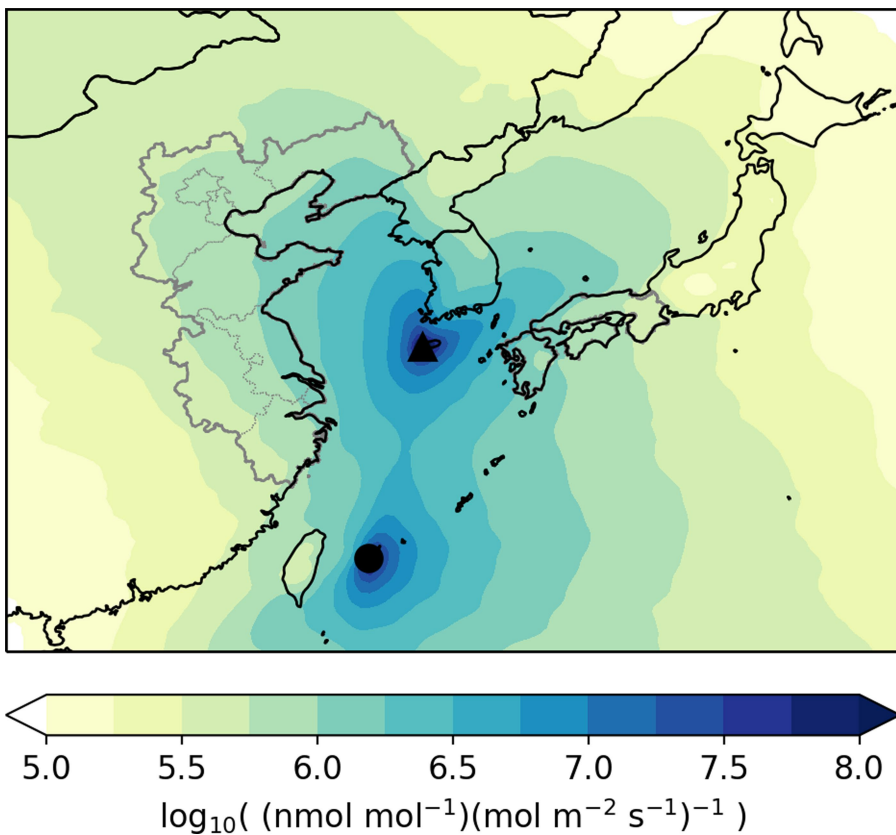
The inversion models of NAME-HB, NAME-InTEM, FLEXPART-MIT and FLEXPART-Empa are used to determine the regional CFC-11 emissions. Enquiries about the model codes should be directed to M.R., A.J.M., S.R. and R.G.P. Licences to use NAME and InTEM are available for research purposes via a request to the UK Met Office or on request from A.J.M. and A.L.R. The code for the NAME-based hierarchical Bayesian inversion (NAME-HB) is available on request from M.R. and L.M.W. The code of the dispersion model FLEXPART is available from www.flexpart.eu. The code for the FLEXPART-based Bayesian inversion (FLEXPART-MIT) is available on request from X.F. The inversion code used by Empa is available from <https://doi.org/10.5281/zenodo.1194642> or on request from S.H.

24. Miller, B. R. et al. Medusa: a sample preconcentration and GC/MS detector system for in situ measurements of atmospheric trace halocarbons, hydrocarbons, and sulfur compounds. *Anal. Chem.* **80**, 1536–1545 (2008).
25. Enomoto, T., Yokouchi, Y., Izumi, K. & Inagaki, T. Development of an analytical method for atmospheric halocarbons and its application to airborne observation. *Jpn. Soc. Atmospheric Environ.* **40**, 1–8 (2005).
26. Cullen, M. J. P. The Unified Forecast/Climate Model. *Meteorol. Mag.* **122**, 81–94 (1993).
27. Chipperfield, M. P. et al. Multimodel estimates of atmospheric lifetimes of long-lived ozone-depleting substances: present and future. *J. Geophys. Res.* **119**, 2555–2573 (2014).
28. Ganeshan, A. L. et al. Characterization of uncertainties in atmospheric trace gas inversions using hierarchical Bayesian methods. *Atmos. Chem. Phys.* **14**, 3855–3864 (2014).
29. Green, P. J. Reversible jump Markov chain Monte Carlo computation and Bayesian model determination. *Biometrika* **82**, 711–732 (1995).
30. Stohl, A. et al. An analytical inversion method for determining regional and global emissions of greenhouse gases: sensitivity studies and application to halocarbons. *Atmos. Chem. Phys.* **9**, 1597–1620 (2009).
31. O'Doherty, S. et al. In situ chloroform measurements at Advanced Global Atmospheric Gases Experiment atmospheric research stations from 1994 to 1998. *J. Geophys. Res.* **106**, 20429–20444 (2001).
32. Rigby, M. et al. Re-evaluation of the lifetimes of the major CFCs and CH_3CCl_3 using atmospheric trends. *Atmos. Chem. Phys.* **13**, 2691–2702 (2013).
33. Rigby, M. et al. Recent and future trends in synthetic greenhouse gas radiative forcing. *Geophys. Res. Lett.* **41**, 2623–2630 (2014).



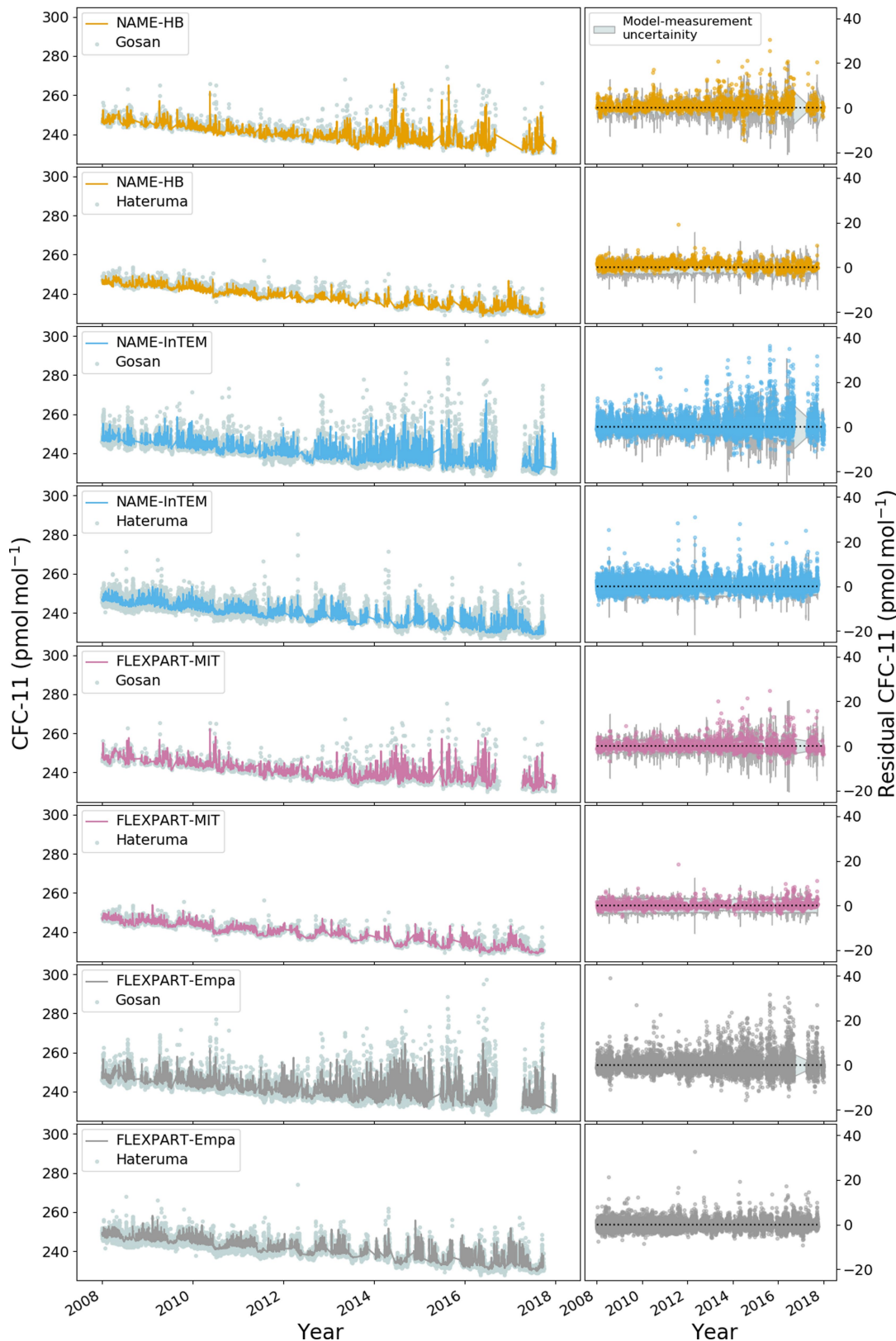
Extended Data Fig. 1 | CFC-11 mole fractions measured at different sites in the AGAGE network and at affiliated sites. Box plots indicate the 25th and 75th of the individual measurement data (approximately 2-hourly), with the median shown as a horizontal line within each box. The whiskers show the 10th and 90th percentiles. The lower percentiles

are typically representative of baseline ('unpolluted') mole fractions, and the difference between the lower and higher percentiles indicates the magnitude of above-baseline events due to the interception of air masses containing recently emitted CFC-11.



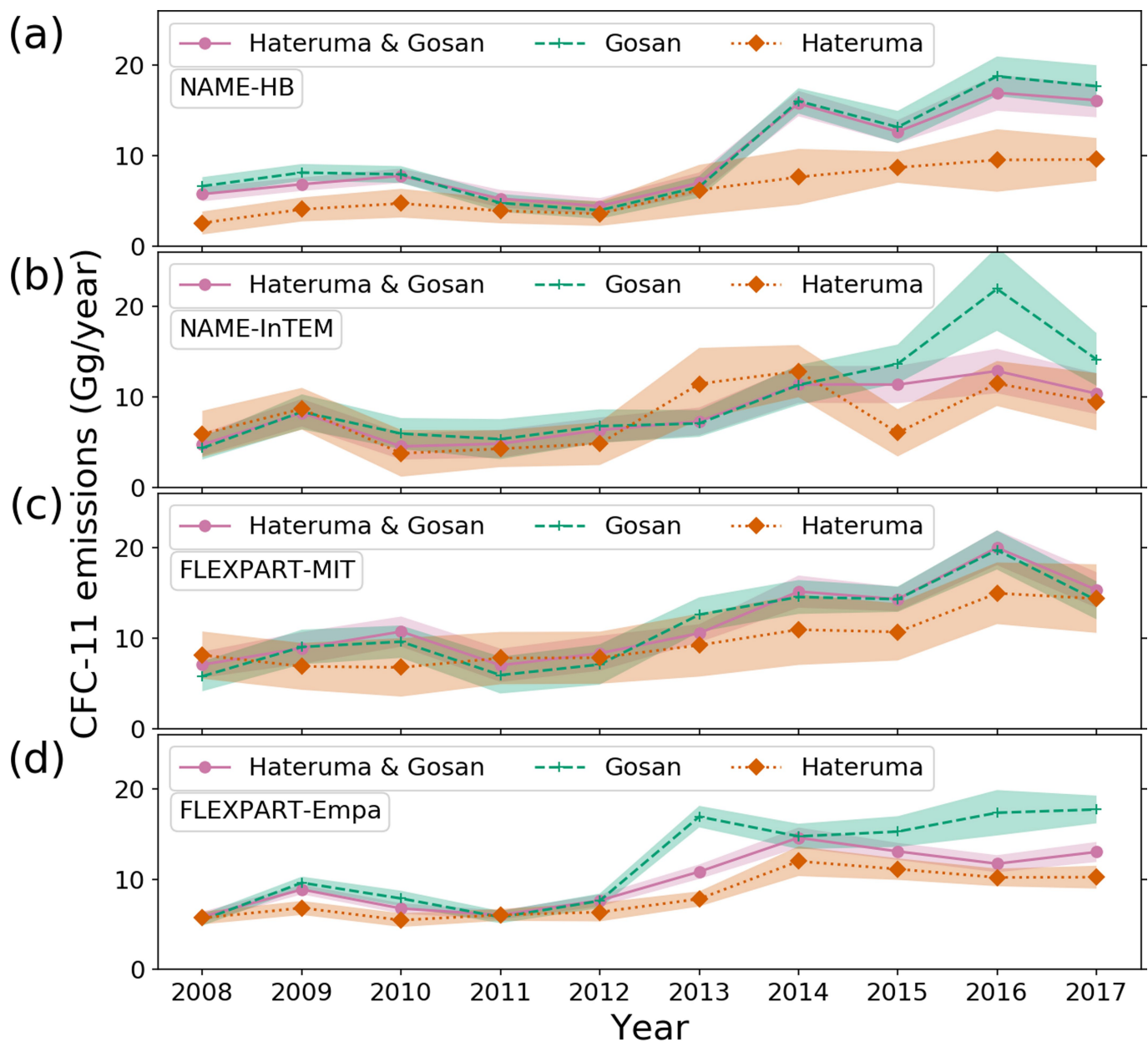
Extended Data Fig. 2 | NAME-derived mean sensitivities of atmospheric mole fractions at Gosan and Hateruma to potential emission. This mean sensitivity map was derived for sampling events at these two sites during 2008 to 2017. Black triangle and circle indicate the Gosan and Hateruma stations, respectively. Thin grey lines show the boundaries of the provinces

within the region we denote eastern mainland China. This region contains the provinces Anhui, Beijing, Hebei, Jiangsu, Liaoning, Shandong, Shanghai, Tianjin and Zhejiang. The west of the grey line transecting Japan, containing the regions Chūgoku, Kansai, Kyūshū & Okinawa, and Shikoku, is the region we denote western Japan.


Extended Data Fig. 3 | Simulated and observed CFC-11 mole fractions

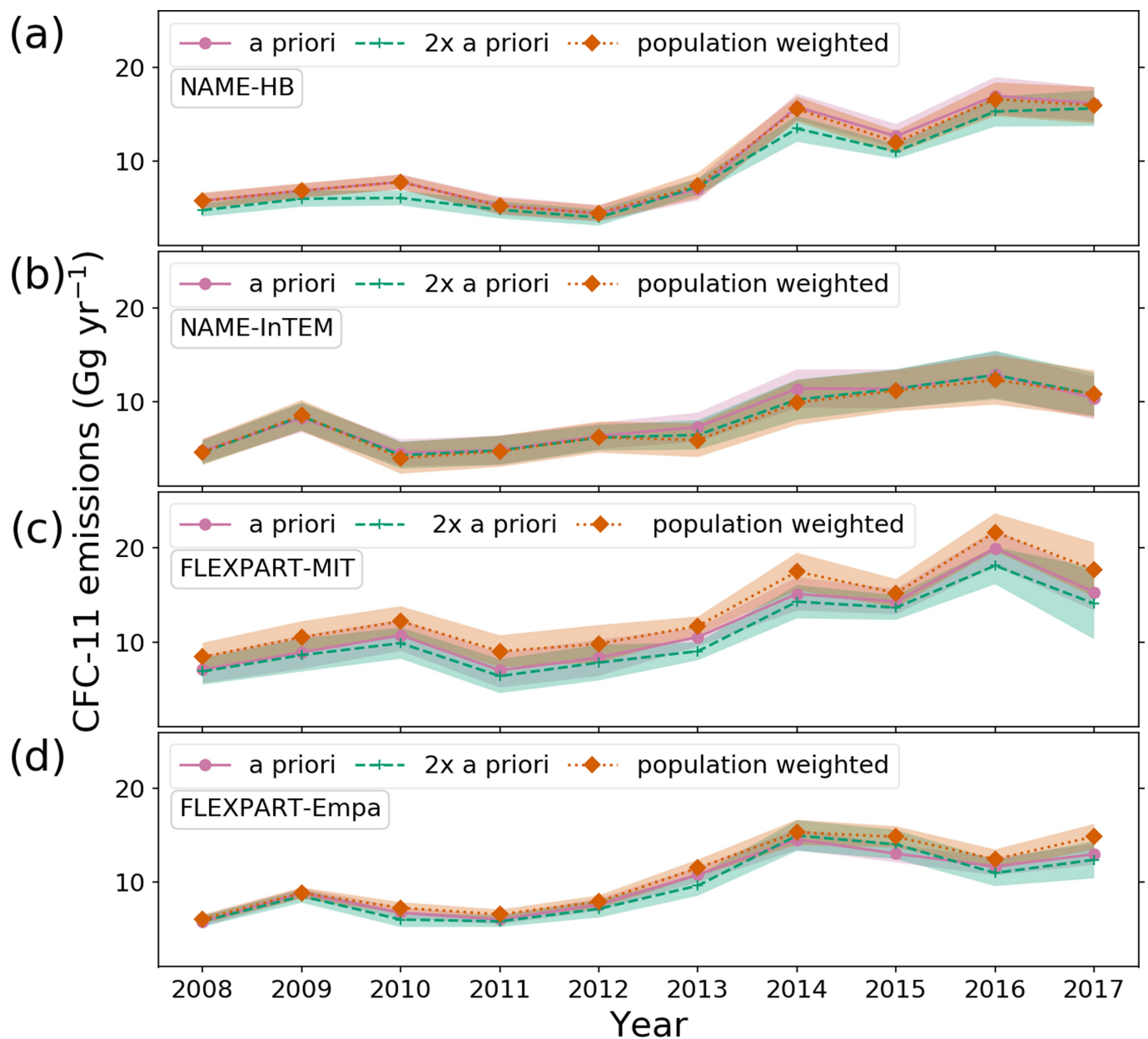
at Gosan and Hateruma. Left, a comparison of the simulated CFC-11 mole fractions from the four different inversion analyses and those that were measured at Gosan and Hateruma. Right, residuals between the simulated and observed mole fractions (data minus model). Shading

denotes 1 s.d. of the model-data mismatch uncertainties assumed in the inversions. Simulated mole fractions are derived from the a posteriori emissions. For the NAME-InTEM, FLEXPART-EMPA, NAME-HB and FLEXPART-MIT inversions, 2-hourly, 3-hourly, 24-hourly and 24-hourly averaging was applied to the model and data, respectively.



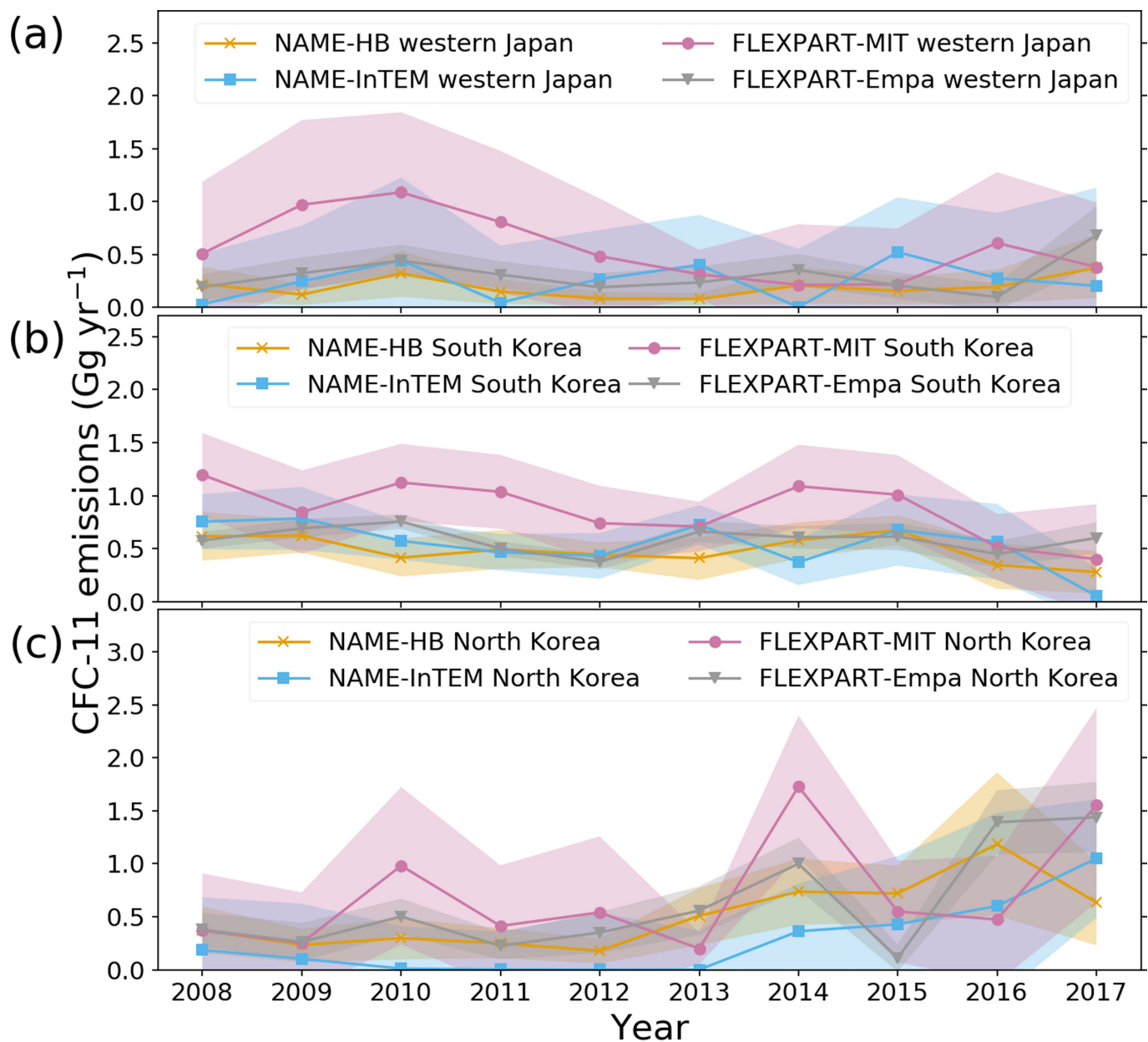
Extended Data Fig. 4 | Derived emissions from different inverse models considering subsets of measurement data. Shown are emission estimates derived using the Gosan CFC-11 measurements (green dashed line), the Hateruma CFC-11 measurements (red dotted line), or both records

in the inversion analysis (pink solid line). **a–d**, Estimates shown use the NAME-HB (a), NAME-InTEM (b), FLEXPART-MIT (c) and FLEXPART-Empa (d) inversion techniques.



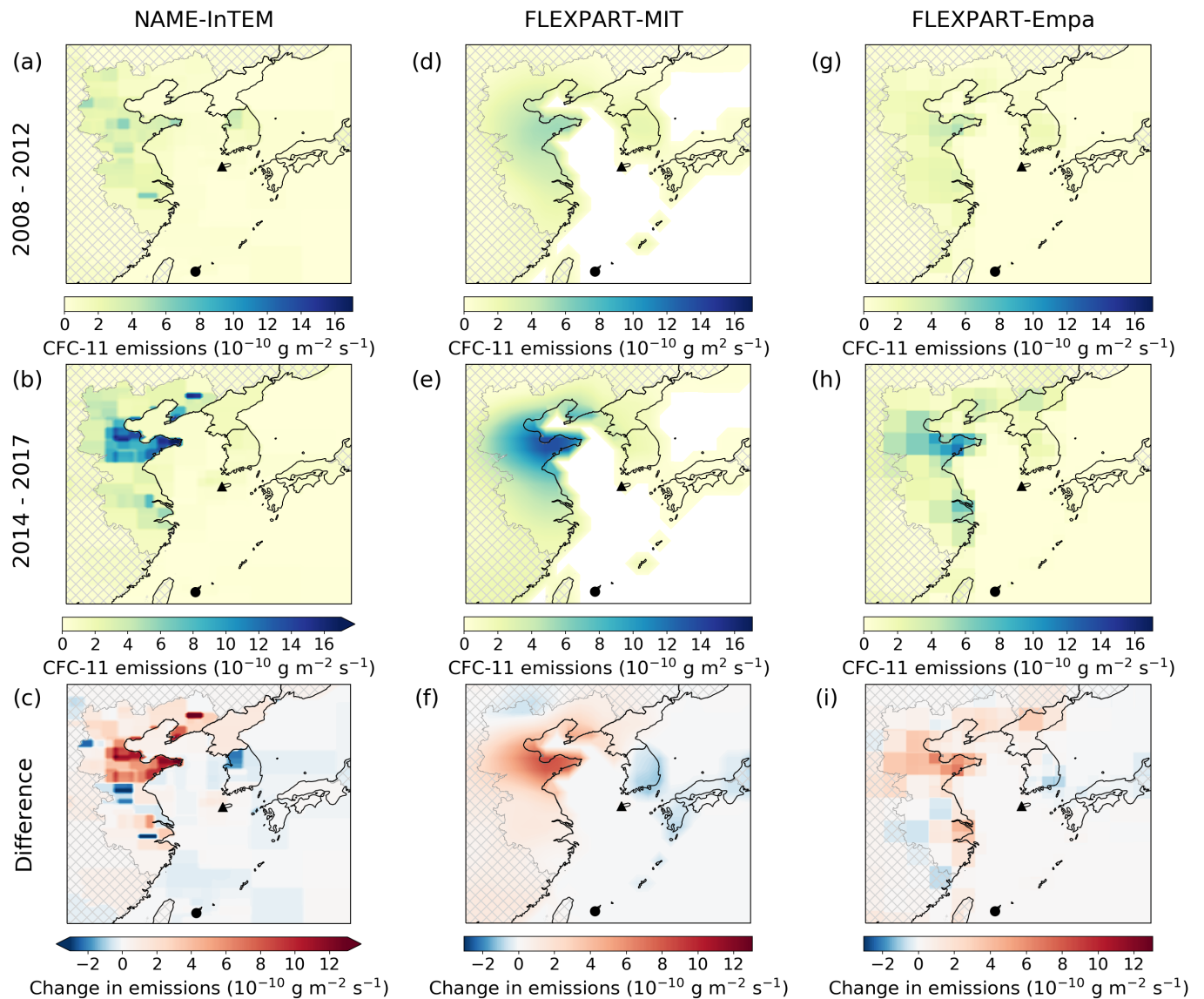
Extended Data Fig. 5 | Derived emissions for eastern mainland China for different a priori emission magnitudes and different spatial distributions. The inversions are as described in Methods ('a priori', pink solid line), with a priori emissions twice as high ('2× a priori', green

dashed line), or the same magnitude but distributed in space according to population density ('population weighted', red dotted line). **a–d**, Estimates shown use the NAME-HB (a), NAME-InTEM (b), FLEXPART-MIT (c) and FLEXPART-Empa (d) inversion methods.



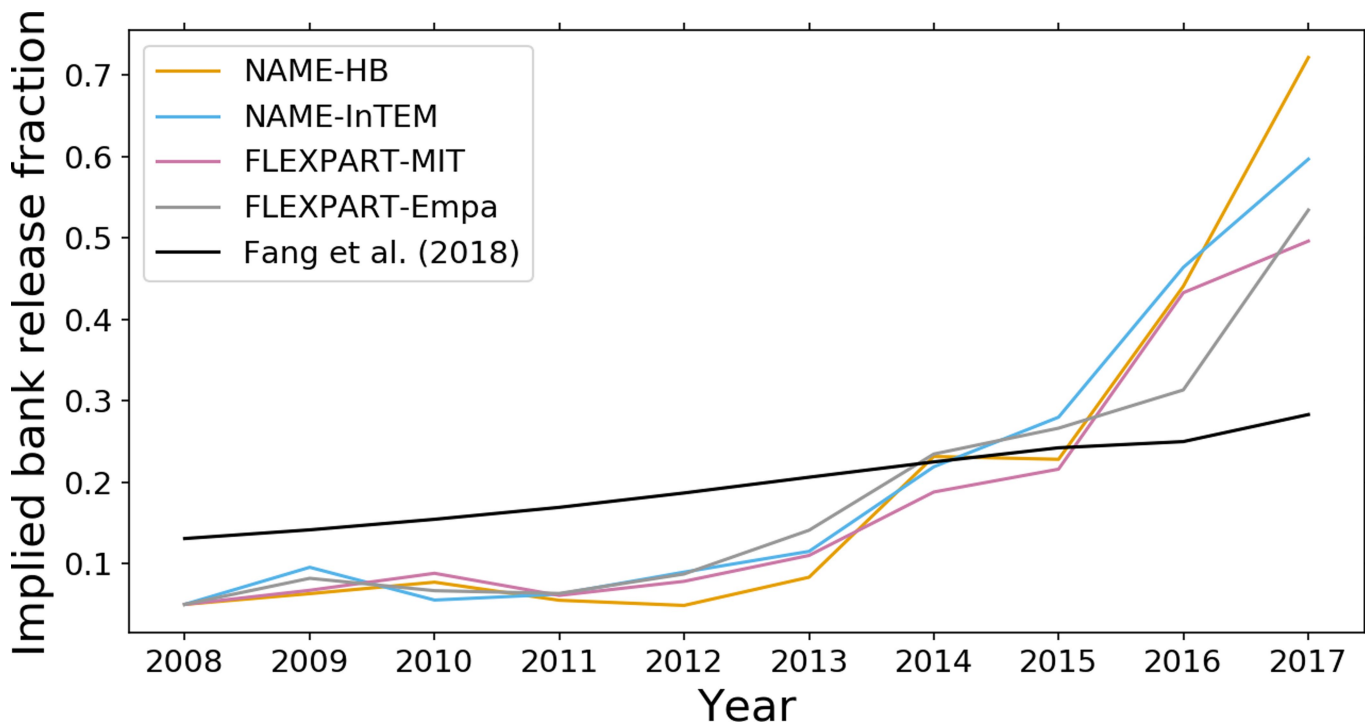
Extended Data Fig. 6 | Top-down CFC-11 emissions estimates in eastern Asia. a–c, Emission estimates are shown for western Japan (a), South Korea (b) and North Korea (c) using the NAME-HB (yellow lines), NAME-InTEM (blue lines), FLEXPART-MIT (pink lines) and FLEXPART-

Empa (grey lines) inverse frameworks described in the Methods. See Extended Data Fig. 2 for the definition of the western Japan region. All lines and symbols are the a posteriori mean, and shading denotes s.d. uncertainty.



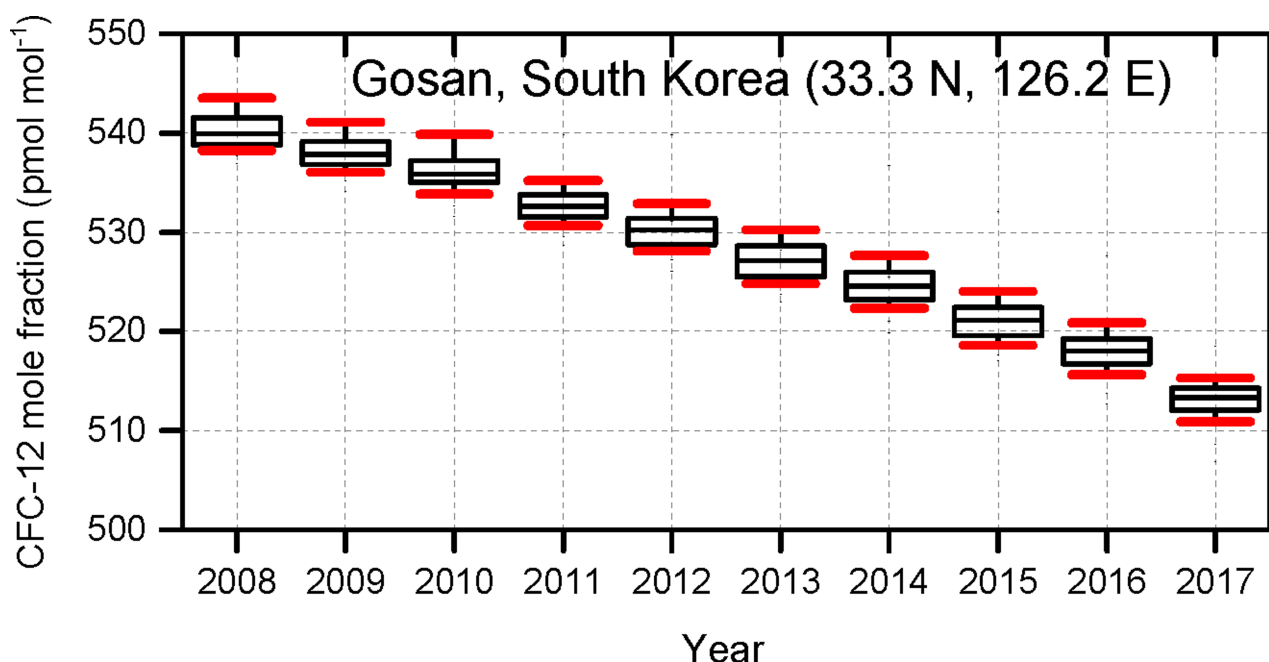
Extended Data Fig. 7 | Maps of mean CFC-11 emission fluxes from different models and time periods, and the differences between time periods. **a–i**, CFC-11 emissions for NAME-InTEM (**a–c**), FLEXPART-MIT (**d–f**) and FLEXPART-Empa (**g–i**) using the inversion framework described in the Methods, and similar to Fig. 3. **a, d, g**, Average spatial

emissions are shown for the period 2008–2012. **b, e, h**, Average spatial emissions are shown for the period 2014–2017. **c, f, i**, The difference in emissions from the 2008–2012 period to the 2013–2017 period, using NAME-InTEM, FLEXPART-MIT and FLEXPART-Empa, respectively.



Extended Data Fig. 8 | The implied bank release fraction of CFC-11 from eastern mainland China. The implied release fraction of banks of CFC-11 from the eastern mainland China region defined in Extended Data Fig. 2, assuming that there is no non-reported production after 2008. This calculation assumes that the 2008 emissions estimates are 5% of the bank size (estimated to be towards the upper limit of expected global

bank fractional release rate³). The coloured lines show the implied bank release fraction for each year after 2008, required to sustain the mean a posteriori emissions from the NAME-HB (yellow), NAME-InTEM (blue), FLEXPART-MIT (pink) and FLEXPART-Empa (grey) inversions. The black line shows the bank release fraction from a bottom-up study for the whole of China⁷.



Extended Data Fig. 9 | CFC-12 mole fractions at the Gosan measurement site. Measured mole fractions of CFC-12 at Gosan, South Korea, from 2008 to 2017. Box plots are as defined in Extended Data Fig. 1.

Reporting Summary

Nature Research wishes to improve the reproducibility of the work that we publish. This form provides structure for consistency and transparency in reporting. For further information on Nature Research policies, see [Authors & Referees](#) and the [Editorial Policy Checklist](#).

Statistics

For all statistical analyses, confirm that the following items are present in the figure legend, table legend, main text, or Methods section.

n/a Confirmed

- The exact sample size (n) for each experimental group/condition, given as a discrete number and unit of measurement
- A statement on whether measurements were taken from distinct samples or whether the same sample was measured repeatedly
- The statistical test(s) used AND whether they are one- or two-sided
Only common tests should be described solely by name; describe more complex techniques in the Methods section.
- A description of all covariates tested
- A description of any assumptions or corrections, such as tests of normality and adjustment for multiple comparisons
- A full description of the statistical parameters including central tendency (e.g. means) or other basic estimates (e.g. regression coefficient) AND variation (e.g. standard deviation) or associated estimates of uncertainty (e.g. confidence intervals)
- For null hypothesis testing, the test statistic (e.g. F , t , r) with confidence intervals, effect sizes, degrees of freedom and P value noted
Give P values as exact values whenever suitable.
- For Bayesian analysis, information on the choice of priors and Markov chain Monte Carlo settings
- For hierarchical and complex designs, identification of the appropriate level for tests and full reporting of outcomes
- Estimates of effect sizes (e.g. Cohen's d , Pearson's r), indicating how they were calculated

Our web collection on [statistics for biologists](#) contains articles on many of the points above.

Software and code

Policy information about [availability of computer code](#)

Data collection

Provide a description of all commercial, open source and custom code used to collect the data in this study, specifying the version used OR state that no software was used.

Data analysis

*The inversion models of NAME-HB, NAME-InTEM, FLEXPART-MIT and FLEXPART-Empa are used to determine the regional CFC-11 emissions. Enquiries about the model codes should be directed to M.R., A.J.M., S.R. and R.G.P. Licences to use NAME and InTEM are available for research purposes via a request to the UK Met Office or on request from A.J.M. and A.I.R. *e.version used*. The code for the NAME-based hierarchical Bayesian inversion (NAME-HB) is available on request from M.R. and L.M.W. The code of the dispersion model FLEXPART is available from www.flexpart.eu. The code for the FLEXPART-based Bayesian inversion (FLEXPART-MIT) is available on request from X.F.. The inversion code used by Empa is available from <https://doi.org/10.5281/zenodo.1194642> or on request from S.H..*

For manuscripts utilizing custom algorithms or software that are central to the research but not yet described in published literature, software must be made available to editors/reviewers. We strongly encourage code deposition in a community repository (e.g. GitHub). See the Nature Research [guidelines for submitting code & software](#) for further information.

Data

Policy information about [availability of data](#)

All manuscripts must include a [data availability statement](#). This statement should provide the following information, where applicable:

- Accession codes, unique identifiers, or web links for publicly available datasets
- A list of figures that have associated raw data
- A description of any restrictions on data availability

 Data from remote AGAGE stations and Gosan data are available from the AGAGE website (agage.mit.edu). Hateruma data are available at World Data Center for Greenhouse Gases (<http://ds.data.jma.go.jp/gmd/wdcgg/wdcgg.html>). NOAA data are taken as the "combined set" data record (a best-estimate record based on flask samples and in-situ measurements), available from the NOAA Global Monitoring Division data server (<https://www.esrl.noaa.gov/gmd/dv/ftpdata.html>, or more specifically <ftp://ftp.cmdl.noaa.gov/hats/cfc11/combined/>)

Field-specific reporting

Please select the one below that is the best fit for your research. If you are not sure, read the appropriate sections before making your selection.

- Life sciences Behavioural & social sciences Ecological, evolutionary & environmental sciences

For a reference copy of the document with all sections, see nature.com/documents/nr-reporting-summary-flat.pdf

Life sciences study design

All studies must disclose on these points even when the disclosure is negative.

Sample size	<i>Describe how sample size was determined, detailing any statistical methods used to predetermine sample size OR if no sample-size calculation was performed, describe how sample sizes were chosen and provide a rationale for why these sample sizes are sufficient.</i>
Data exclusions	<i>Describe any data exclusions. If no data were excluded from the analyses, state so OR if data were excluded, describe the exclusions and the rationale behind them, indicating whether exclusion criteria were pre-established.</i>
Replication	<i>Describe the measures taken to verify the reproducibility of the experimental findings. If all attempts at replication were successful, confirm this OR if there are any findings that were not replicated or cannot be reproduced, note this and describe why.</i>
Randomization	<i>Describe how samples/organisms/participants were allocated into experimental groups. If allocation was not random, describe how covariates were controlled OR if this is not relevant to your study, explain why.</i>
Blinding	<i>Describe whether the investigators were blinded to group allocation during data collection and/or analysis. If blinding was not possible, describe why OR explain why blinding was not relevant to your study.</i>

Behavioural & social sciences study design

All studies must disclose on these points even when the disclosure is negative.

Study description	<i>Briefly describe the study type including whether data are quantitative, qualitative, or mixed-methods (e.g. qualitative cross-sectional, quantitative experimental, mixed-methods case study).</i>
Research sample	<i>State the research sample (e.g. Harvard university undergraduates, villagers in rural India) and provide relevant demographic information (e.g. age, sex) and indicate whether the sample is representative. Provide a rationale for the study sample chosen. For studies involving existing datasets, please describe the dataset and source.</i>
Sampling strategy	<i>Describe the sampling procedure (e.g. random, snowball, stratified, convenience). Describe the statistical methods that were used to predetermine sample size OR if no sample-size calculation was performed, describe how sample sizes were chosen and provide a rationale for why these sample sizes are sufficient. For qualitative data, please indicate whether data saturation was considered, and what criteria were used to decide that no further sampling was needed.</i>
Data collection	<i>Provide details about the data collection procedure, including the instruments or devices used to record the data (e.g. pen and paper, computer, eye tracker, video or audio equipment) whether anyone was present besides the participant(s) and the researcher, and whether the researcher was blind to experimental condition and/or the study hypothesis during data collection.</i>
Timing	<i>Indicate the start and stop dates of data collection. If there is a gap between collection periods, state the dates for each sample cohort.</i>
Data exclusions	<i>If no data were excluded from the analyses, state so OR if data were excluded, provide the exact number of exclusions and the rationale behind them, indicating whether exclusion criteria were pre-established.</i>
Non-participation	<i>State how many participants dropped out/declined participation and the reason(s) given OR provide response rate OR state that no participants dropped out/declined participation.</i>
Randomization	<i>If participants were not allocated into experimental groups, state so OR describe how participants were allocated to groups, and if allocation was not random, describe how covariates were controlled.</i>

Ecological, evolutionary & environmental sciences study design

All studies must disclose on these points even when the disclosure is negative.

Study description	<i>Briefly describe the study. For quantitative data include treatment factors and interactions, design structure (e.g. factorial, nested, hierarchical), nature and number of experimental units and replicates.</i>
Research sample	<i>Describe the research sample (e.g. a group of tagged <i>Passer domesticus</i>, all <i>Stenocereus thurberi</i> within Organ Pipe Cactus National Monument), and provide a rationale for the sample choice. When relevant, describe the organism taxa, source, sex, age range and any manipulations. State what population the sample is meant to represent when applicable. For studies involving existing datasets, describe the data and its source.</i>
Sampling strategy	<i>Note the sampling procedure. Describe the statistical methods that were used to predetermine sample size OR if no sample-size calculation was performed, describe how sample sizes were chosen and provide a rationale for why these sample sizes are sufficient.</i>

Data collection	Describe the data collection procedure, including who recorded the data and how.
Timing and spatial scale	Indicate the start and stop dates of data collection, noting the frequency and periodicity of sampling and providing a rationale for these choices. If there is a gap between collection periods, state the dates for each sample cohort. Specify the spatial scale from which the data are taken
Data exclusions	If no data were excluded from the analyses, state so OR if data were excluded, describe the exclusions and the rationale behind them, indicating whether exclusion criteria were pre-established.
Reproducibility	Describe the measures taken to verify the reproducibility of experimental findings. For each experiment, note whether any attempts to repeat the experiment failed OR state that all attempts to repeat the experiment were successful.
Randomization	Describe how samples/organisms/participants were allocated into groups. If allocation was not random, describe how covariates were controlled. If this is not relevant to your study, explain why.
Blinding	Describe the extent of blinding used during data acquisition and analysis. If blinding was not possible, describe why OR explain why blinding was not relevant to your study.

Did the study involve field work? Yes No

Field work, collection and transport

Field conditions	Describe the study conditions for field work, providing relevant parameters (e.g. temperature, rainfall).
Location	State the location of the sampling or experiment, providing relevant parameters (e.g. latitude and longitude, elevation, water depth).
Access and import/export	Describe the efforts you have made to access habitats and to collect and import/export your samples in a responsible manner and in compliance with local, national and international laws, noting any permits that were obtained (give the name of the issuing authority, the date of issue, and any identifying information).
Disturbance	Describe any disturbance caused by the study and how it was minimized.

Reporting for specific materials, systems and methods

We require information from authors about some types of materials, experimental systems and methods used in many studies. Here, indicate whether each material, system or method listed is relevant to your study. If you are not sure if a list item applies to your research, read the appropriate section before selecting a response.

Materials & experimental systems		Methods	
n/a	Involved in the study	n/a	Involved in the study
<input checked="" type="checkbox"/>	<input type="checkbox"/> Antibodies	<input checked="" type="checkbox"/>	<input type="checkbox"/> ChIP-seq
<input checked="" type="checkbox"/>	<input type="checkbox"/> Eukaryotic cell lines	<input checked="" type="checkbox"/>	<input type="checkbox"/> Flow cytometry
<input checked="" type="checkbox"/>	<input type="checkbox"/> Palaeontology	<input checked="" type="checkbox"/>	<input type="checkbox"/> MRI-based neuroimaging
<input checked="" type="checkbox"/>	<input type="checkbox"/> Animals and other organisms		
<input checked="" type="checkbox"/>	<input type="checkbox"/> Human research participants		
<input checked="" type="checkbox"/>	<input type="checkbox"/> Clinical data		

Antibodies

Antibodies used	Describe all antibodies used in the study; as applicable, provide supplier name, catalog number, clone name, and lot number.
Validation	Describe the validation of each primary antibody for the species and application, noting any validation statements on the manufacturer's website, relevant citations, antibody profiles in online databases, or data provided in the manuscript.

Eukaryotic cell lines

Policy information about cell lines	
Cell line source(s)	State the source of each cell line used.
Authentication	Describe the authentication procedures for each cell line used OR declare that none of the cell lines used were authenticated.
Mycoplasma contamination	Confirm that all cell lines tested negative for mycoplasma contamination OR describe the results of the testing for mycoplasma contamination OR declare that the cell lines were not tested for mycoplasma contamination.

Commonly misidentified lines
(See [ICLAC](#) register)

Name any commonly misidentified cell lines used in the study and provide a rationale for their use.

Palaeontology

Specimen provenance	Provide provenance information for specimens and describe permits that were obtained for the work (including the name of the issuing authority, the date of issue, and any identifying information).
Specimen deposition	Indicate where the specimens have been deposited to permit free access by other researchers.
Dating methods	If new dates are provided, describe how they were obtained (e.g. collection, storage, sample pretreatment and measurement), where they were obtained (i.e. lab name), the calibration program and the protocol for quality assurance OR state that no new dates are provided.

Tick this box to confirm that the raw and calibrated dates are available in the paper or in Supplementary Information.

Animals and other organisms

Policy information about [studies involving animals; ARRIVE guidelines](#) recommended for reporting animal research

Laboratory animals	For laboratory animals, report species, strain, sex and age OR state that the study did not involve laboratory animals.
Wild animals	Provide details on animals observed in or captured in the field; report species, sex and age where possible. Describe how animals were caught and transported and what happened to captive animals after the study (if killed, explain why and describe method; if released, say where and when) OR state that the study did not involve wild animals.
Field-collected samples	For laboratory work with field-collected samples, describe all relevant parameters such as housing, maintenance, temperature, photoperiod and end-of-experiment protocol OR state that the study did not involve samples collected from the field.
Ethics oversight	Identify the organization(s) that approved or provided guidance on the study protocol, OR state that no ethical approval or guidance was required and explain why not.

Note that full information on the approval of the study protocol must also be provided in the manuscript.

Human research participants

Policy information about [studies involving human research participants](#)

Population characteristics	Describe the covariate-relevant population characteristics of the human research participants (e.g. age, gender, genotypic information, past and current diagnosis and treatment categories). If you filled out the behavioural & social sciences study design questions and have nothing to add here, write "See above."
Recruitment	Describe how participants were recruited. Outline any potential self-selection bias or other biases that may be present and how these are likely to impact results.
Ethics oversight	Identify the organization(s) that approved the study protocol.

Note that full information on the approval of the study protocol must also be provided in the manuscript.

Clinical data

Policy information about [clinical studies](#)

All manuscripts should comply with the ICMJE [guidelines for publication of clinical research](#) and a completed [CONSORT checklist](#) must be included with all submissions.

Clinical trial registration	Provide the trial registration number from ClinicalTrials.gov or an equivalent agency.
Study protocol	Note where the full trial protocol can be accessed OR if not available, explain why.
Data collection	Describe the settings and locales of data collection, noting the time periods of recruitment and data collection.
Outcomes	Describe how you pre-defined primary and secondary outcome measures and how you assessed these measures.

ChIP-seq

Data deposition

- Confirm that both raw and final processed data have been deposited in a public database such as [GEO](#).
- Confirm that you have deposited or provided access to graph files (e.g. BED files) for the called peaks.

Data access links <i>May remain private before publication.</i>	For "Initial submission" or "Revised version" documents, provide reviewer access links. For your "Final submission" document, provide a link to the deposited data.
Files in database submission	Provide a list of all files available in the database submission.
Genome browser session (e.g. UCSC)	Provide a link to an anonymized genome browser session for "Initial submission" and "Revised version" documents only, to enable peer review. Write "no longer applicable" for "Final submission" documents.

Methodology

Replicates	Describe the experimental replicates, specifying number, type and replicate agreement.
Sequencing depth	Describe the sequencing depth for each experiment, providing the total number of reads, uniquely mapped reads, length of reads and whether they were paired- or single-end.
Antibodies	Describe the antibodies used for the ChIP-seq experiments; as applicable, provide supplier name, catalog number, clone name, and lot number.
Peak calling parameters	Specify the command line program and parameters used for read mapping and peak calling, including the ChIP, control and index files used.
Data quality	Describe the methods used to ensure data quality in full detail, including how many peaks are at FDR 5% and above 5-fold enrichment.
Software	Describe the software used to collect and analyze the ChIP-seq data. For custom code that has been deposited into a community repository, provide accession details.

Flow Cytometry

Plots

Confirm that:

- The axis labels state the marker and fluorochrome used (e.g. CD4-FITC).
- The axis scales are clearly visible. Include numbers along axes only for bottom left plot of group (a 'group' is an analysis of identical markers).
- All plots are contour plots with outliers or pseudocolor plots.
- A numerical value for number of cells or percentage (with statistics) is provided.

Methodology

Sample preparation	Describe the sample preparation, detailing the biological source of the cells and any tissue processing steps used.
Instrument	Identify the instrument used for data collection, specifying make and model number.
Software	Describe the software used to collect and analyze the flow cytometry data. For custom code that has been deposited into a community repository, provide accession details.
Cell population abundance	Describe the abundance of the relevant cell populations within post-sort fractions, providing details on the purity of the samples and how it was determined.
Gating strategy	Describe the gating strategy used for all relevant experiments, specifying the preliminary FSC/SSC gates of the starting cell population, indicating where boundaries between "positive" and "negative" staining cell populations are defined.

Tick this box to confirm that a figure exemplifying the gating strategy is provided in the Supplementary Information.

Magnetic resonance imaging

Experimental design

Design type	Indicate task or resting state; event-related or block design.
Design specifications	Specify the number of blocks, trials or experimental units per session and/or subject, and specify the length of each trial or block (if trials are blocked) and interval between trials.
Behavioral performance measures	State number and/or type of variables recorded (e.g. correct button press, response time) and what statistics were used to establish that the subjects were performing the task as expected (e.g. mean, range, and/or standard deviation across subjects).

Acquisition

Imaging type(s)	Specify: functional, structural, diffusion, perfusion.	
Field strength	Specify in Tesla	
Sequence & imaging parameters	Specify the pulse sequence type (gradient echo, spin echo, etc.), imaging type (EPI, spiral, etc.), field of view, matrix size, slice thickness, orientation and TE/TR/flip angle.	
Area of acquisition	State whether a whole brain scan was used OR define the area of acquisition, describing how the region was determined.	
Diffusion MRI	<input type="checkbox"/> Used	<input type="checkbox"/> Not used

Preprocessing

Preprocessing software	Provide detail on software version and revision number and on specific parameters (model/functions, brain extraction, segmentation, smoothing kernel size, etc.).	
Normalization	If data were normalized/standardized, describe the approach(es): specify linear or non-linear and define image types used for transformation OR indicate that data were not normalized and explain rationale for lack of normalization.	
Normalization template	Describe the template used for normalization/transformation, specifying subject space or group standardized space (e.g. original Talairach, MNI305, ICBM152) OR indicate that the data were not normalized.	
Noise and artifact removal	Describe your procedure(s) for artifact and structured noise removal, specifying motion parameters, tissue signals and physiological signals (heart rate, respiration).	
Volume censoring	Define your software and/or method and criteria for volume censoring, and state the extent of such censoring.	

Statistical modeling & inference

Model type and settings	Specify type (mass univariate, multivariate, RSA, predictive, etc.) and describe essential details of the model at the first and second levels (e.g. fixed, random or mixed effects; drift or auto-correlation).	
Effect(s) tested	Define precise effect in terms of the task or stimulus conditions instead of psychological concepts and indicate whether ANOVA or factorial designs were used.	
Specify type of analysis:	<input type="checkbox"/> Whole brain	<input type="checkbox"/> ROI-based
Statistic type for inference (See Eklund et al. 2016)	Specify voxel-wise or cluster-wise and report all relevant parameters for cluster-wise methods.	
Correction	Describe the type of correction and how it is obtained for multiple comparisons (e.g. FWE, FDR, permutation or Monte Carlo).	

Models & analysis

n/a	Involved in the study	
<input type="checkbox"/>	<input type="checkbox"/> Functional and/or effective connectivity	
<input type="checkbox"/>	<input type="checkbox"/> Graph analysis	
<input type="checkbox"/>	<input type="checkbox"/> Multivariate modeling or predictive analysis	
Functional and/or effective connectivity	Report the measures of dependence used and the model details (e.g. Pearson correlation, partial correlation, mutual information).	
Graph analysis	Report the dependent variable and connectivity measure, specifying weighted graph or binarized graph, subject- or group-level, and the global and/or node summaries used (e.g. clustering coefficient, efficiency, etc.).	
Multivariate modeling and predictive analysis	Specify independent variables, features extraction and dimension reduction, model, training and evaluation metrics.	